HHS Public Access

Author manuscript

Proc SPIE Int Soc Opt Eng. Author manuscript; available in PMC 2010 April 20.

Published in final edited form as:

Proc SPIE Int Soc Opt Eng. 2009 January 1; 7259: . doi:10.1117/12.811610.

Brain Tissue Segmentation of Neonatal MR Images Using a Longitudinal Subject-specific Probabilistic Atlas

Feng Shi[a], **Yong Fan**[a], **Songyuan Tang**[a], **John Gilmore**[c], **Weili Lin**[b], and **Dinggang Shen**[a]

[a]IDEA Lab, Department of Radiology and BRIC, University of North Carolina at Chapel Hill

[b]MRI Lab, Department of Radiology and BRIC, University of North Carolina at Chapel Hill

[c]Department of Psychiatry, University of North Carolina at Chapel Hill

Abstract

Brain tissue segmentation of neonate MR images is a challenging task in study of early brain development, due to low signal contrast among brain tissues and high intensity variability especially in white matter. Among various brain tissue segmentation algorithms, the atlas-based segmentation techniques can potentially produce reasonable segmentation results on neonatal brain images. However, their performance on the population-based atlas is still limited due to the high variability of brain structures across different individuals. Moreover, it may be impossible to generate a reasonable probabilistic atlas for neonates without tissue segmentation samples. To overcome these limitations, we present a neonatal brain tissue segmentation method by taking advantage of the longitudinal data available in our study to establish a subject-specific probabilistic atlas. In particular, tissue segmentation of the neonatal brain is formulated as two iterative steps of bias correction and probabilistic atlas based tissue segmentation, along with the guidance of brain tissue segmentation resulted from the later time images of the same subject which serve as a subject-specific probabilistic atlas. The proposed method has been evaluated qualitatively through visual inspection and quantitatively by comparing with manual delineation results. Experimental results show that the utilization of a subject-specific probabilistic atlas can substantially improve tissue segmentation of neonatal brain images.

Keywords

Neonate; Tissue segmentation; Probabilistic atlas; Subject-specific atlas

1. INTRODUCTION

MRI studies in neonates have attracted a lot of research interests in brain development due to its potential to reveal the early brain developing pattern [1-3]. To perform volumetric or cortical surface analysis in the brain, tissue segmentation is a fundamental step, which classifies brain images into gray matter (GM), white matter (WM), and cerebrospinal fluid (CSF). The brain tissue segmentation problem has been well studied for adult brain images [4]. However, it still remains challenging for neonatal brain images, due to the low brain tissue

contrast and poor spatial resolution as compared with adult brain images. Moreover, due to the dynamic WM myelination process, the tissue intensity pattern in the neonatal brain changes dramatically with age. Specifically, the brain is mostly unmyelinated in newborns, but rapidly changes in the first year, and the adult pattern occurs at 2 years of age [5]. The conventional intensity-based segmentation algorithm, which assumes a similar intensity for the same brain tissue, generally fails for the segmentation of neonatal brains due to the large overlap of tissue intensity distributions of GM, WM, and CSF, making it difficult even for experts to distinguish between different neonatal brain tissues [6,7].

To overcome these problems, knowledge-based brain tissue segmentation methods for neonate images have been proposed [6-12], among which the probabilistic atlas based segmentation technique has a potential to yield promising results. In general, the probabilistic atlas is created from a set of previously segmented brain images which have been spatial normalized into a standard space [13-15]. Then, voxel-wise tissue probability in the standard space is estimated from all spatially normalized images. To apply the atlas based techniques to neonate brain image segmentation, one needs to solve the following problems. *First*, the adult brain atlas cannot be directly applied to neonates due to large anatomical difference between the neonatal and the adult brains. Similarly, a general pediatric probabilistic atlas cannot be directly applied because the brain develops dramatically in the first year of life, and brain tissue patterns differ largely between neonates and other ages. *Second*, the probabilistic atlas constructed from a population is generally very fuzzy particularly in the cortical regions, making it difficult to perform high-performance segmentation in the cortex and other sub-cortical regions (see Fig. 1).

On the other hand, it is known that the adult pattern occurs at two years old [5], and the segmentation of the two-year-old or later time brain images is relatively easy with conventional segmentation methods. More importantly, the cortical convolution patterns remain similar after birth. For example, as indicated in Fig. 2, the cortical patterns within the solid (and dashed) circles are very similar across images obtained at two weeks, one year, and two years old of the same subject. Therefore, the segmentation results of the later time images can potentially serve as a subject-specific tissue probabilistic atlas to guide the segmentation of the neonatal brain images from the same subject. In this paper, longitudinal MR images were employed to obtain a longitudinal subject-specific atlas (with high local specificity) for performing accurate tissue segmentation for neonatal brain images. Experimental results will be provided below.

2. METHOD

To take advantage of the longitudinal data acquired in our study, we propose a subject-specific atlas based tissue segmentation method for neonatal brain images. As summarized in Fig. 3, the proposed method is designed to segment brain tissues from longitudinal images acquired at approximately two weeks, one year old, and two years old. It consists of two main steps: (1) the intensity-based segmentation of two-year-old brain images as well as the creation of a subject-specific tissue probabilistic atlas, as described in the right panel of Fig. 3; (2) the probabilistic atlas based tissue segmentation on the images acquired at an earlier time point (such as two weeks or one year old), as described in the left panel of Fig. 3. In

these two segmentation steps, we iteratively performed the bias correction and the intensity or probabilistic atlas based tissue segmentation until convergence. Notice the tissue segmentation results of the one-year-old images can also be used for creating a tissue probabilistic atlas and for combining with the two-year-old tissue probabilistic atlas to generate an integrated atlas for better guiding of the segmentation of two-week images.

In the following subsections, we will describe our proposed segmentation method by first introducing the preprocessing steps for skull-stripping and cerebellum removal, and then detailing the two major steps proposed in our segmentation method.

2.1 Preprocessing step

Skull-stripping is a standard processing step in brain image analysis, which helps improving the performance of subsequent analysis steps. Thus, in our study, all non-brain tissues in the images acquired at each time point were removed by using Brain Surface Extractor (BSE) [16], followed by manual editing to ensure the complete removal of the skull. Moreover, in order to focus on segmenting brain tissues only, we also manually removed the cerebellum in all images. The results of skull-stripped and cerebellum-removed images can be observed in Figs. 1~7.

2.2 Step 1: Segmentation of two-year-old image

For segmenting two-year-old brain images, we performed an iterative procedure of bias correction and intensity-based tissue segmentation. In particular, the nonparametric nonuniform intensity normalization (N3) technique was used to perform bias correction [17]. For brain tissue segmentation, we used the FMRIB's Automated Segmentation Tool (FAST) [18], which uses Markov Random Field for tissue segmentation. The brain images were segmented into three tissue types, i.e., GM, WM, and CSF. The final tissue segmentation results by this iterative procedure are shown in Fig. 4. It is worth noting that the above steps of bias correction and tissue segmentation also generate three tissue probabilistic maps for GM, WM, and CSF, respectively, which can be subsequently used to guide tissue segmentation of the earlier-time images as detailed below.

2.3 Step 2: Probabilistic atlas based segmentation of neonatal image

To segment the images acquired at earlier time points (such as two weeks or one year old), the tissue probabilistic maps of the later-time images were first aligned onto the space of the earlier-time images. This was achieved by linear alignment of the original skull-stripped two-year-old images onto the two-week (or one-year-old) skull-stripped images, and then using the estimated transformation to map the tissue probabilistic atlases onto the same neonatal image space. For example, the obtained atlases in the neonate image space are represented as $\{p(y_i|k), k=\text{WM, GM, CSF}\}$, which can be used as priors to guide the tissue segmentation of the neonate brain as detailed below.

Next, we introduce an iterative procedure of bias correction and probabilistic atlas based segmentation. The bias field was set as homogeneous in the beginning, and it was iteratively updated based on the segmentation result. With the estimated bias field, the intensity non-

uniformity in the neonate images can be corrected, and the resulting bias corrected images can be used for tissue segmentation using an Expectation-Maximization (EM) algorithm.

In the EM algorithm, a Gaussian mixture model (GMM) was first employed to model the intensity distribution of the *k*-th tissue in the neonatal brain images:

$$p\left(y_i|k\right)=\sum_{n=1}^{N_k}\gamma_{k,n}p\left(y_i|k,n\right)=\sum_{n=1}^{N_k}\gamma_{k,n}\frac{1}{\sqrt{2\pi\sigma_{k,n}{}^{n}}}exp\left(-\frac{\left(y_i-\mu_{k,n}\right)^2}{2\sigma_{k,n}^2}\right) \quad (1)$$

where y_i is the intensity of voxel *i*. N_k is the number of Gaussian functions used to estimate the intensity distribution in the *k*-th tissue. $p\ (y_i \mid k, n)$ is the probability density function parameterized with the mean $\mu_{k,n}$ and the variance $\sigma_{k,n}$ of the intensity in the *n*-th Gaussian function of the neonate images. $\gamma_{k,n}$ is a mixing proportion and it sums to one for each tissue *k*.

To estimate the parameters in GMM, the warped probabilistic atlases $\{p(y_i|k)\}$ were applied to the neonate images as prior probability. By incorporating with neonatal image intensity, the posterior probability map is estimated by the Bayes rule. The E-step in the EM algorithm focuses on estimating the *n*-th Gaussian function in the *k*-th tissue:

$$p\left(k,n|y_i\right)=\frac{p\left(y_i|k,n\right)p\left(k,n\right)}{p\left(y_i\right)} \quad (2)$$

where $p(y_i|k, n)$ and $p(k,n)$ are given by the warped probabilistic atlas of the *k*-th tissue. $p(y_i)$ is obtained by GMM with parameters $\{\gamma,\mu,\sigma\}$

After obtained the posterior probability $p(k,n|y_i)$ in the E-step, the new values of parameters γ, μ and σ can be estimated in the M-step as follows:

$$\gamma_{k,n}=\frac{1}{I}\sum_{i=1}^{I}p\left(k,n|y_i\right) \quad (3)$$

$$\mu_{k,n}=\frac{\sum_{i=1}^{t}p\left(k,n|y_i\right)y_i}{\sum_{i=1}^{I}p\left(k,n|y_i\right)} \quad (4)$$

$$\sigma_{k,n}=sqrt\left(\frac{\sum_{i=1}^{I}p\left(k,n|y_i\right)\left(y_i-\mu_{k,n}\right)^2}{\sum_{i=1}^{I}p\left(k,n|y_i\right)}\right) \quad (5)$$

where *I* is the total number of voxels in the neonate images. The EM algorithm as well as the bias correction were iterated until convergence. The final segmentation results were obtained by assigning each voxel with the maximum belonging probability to a certain class.

The probabilistic maps and the final segmentation results of the two-week images are provided in Fig. 5.

It is worth noting that our segmentation algorithm has a certain tolerance to slight errors in the probabilistic atlas. For example, the frontal area in the warped prior probability maps (Fig. 5b-d) is slightly different from that of neonate images (Fig. 5a), while the segmentation is not dominated by prior atlas; instead, it produces reasonable results (Fig. 5e-h).

Considering the tissue intensity contrast is dramatically changed during the brain developmental process, the intensity based registration method may not achieve good registration between neonate and 2-year-old images. To improve registration, we could non-rigidly register them by using their segmented images, particularly after we obtain the tissue segmentation result for the neonate image. We could potentially repeat the probabilistic atlas based tissue segmentation and the non-rigid registration iteratively to achieve better segmentation, as most joint segmentation and registration methods did [19].

3. EXPERIMENTAL RESULTS

To evaluate the proposed segmentation method, we applied it to a dataset of 10 neonates, each with the longitudinal T1-weighted MR images acquired at a mean gestational age of two weeks, one year old, and two years old. All of the scans were performed using a 3T Siemens scanner with the following MR imaging parameters, TR=1900ms, TE=4.38ms, Flip Angle=7, acquisition matrix=256×192, resolution=1×1×1 mm^3, and 160 axial slices.

To visually inspect the segmentation performance, segmentation results of four representative subjects are shown in Fig. 6. In each panel from (a) to (d), the first column shows the original images and the second column shows the segmentation results. In particular, the results in the two-week images are impressive, where all major and even small structures are reasonably segmented.

For quantitative evaluation of our proposed tissue segmentation method, two experts manually segmented 10 subject images in 2 sagittal slices, 3 coronal slices, and 3 transverse slices by using the same initialization for segmentation and the ITK-SNAP software [20]. The manual segmentation was performed on the T2-weighted images, and the segmentation results are rigidly transformed to the T1-weighted images, for allowing the evaluation of tissue segmentation results on the T1-weighted images.

Our neonate segmentation results were compared with manual segmentation results by measuring the overlay percentage and the volume error. The overlay percentage is measured by the Dice ratio (DR) [21]. Considering two segmented regions *A* and *B*, the Dice ratio is defined as follows:

$$DR=\frac{2\times|A\cap B|}{|A|+|B|}$$

The range of DR is from 0 (complete non-overlay) to 1 (perfect overlay). Generally, 0.7 is considered as satisfactory agreement of the two regions [22]. Note that the central brain

region, as shown in Fig. 7, was blocked in manual segmentation due to its low tissue contrast, and thus it is not included in the computation of the Dice ratio in our experiment. The comparison results on the manual and automated segmentations are shown in Fig. 8.

The overall Dice ratios of segmentation results between our proposed method and the two manual raters are, respectively, 0.79±0.02 and 0.76±0.03 for GM, and 0.75±0.04 and 0.73±0.04 for WM. This indicates high agreement between our results and manual segmentation results in both GM and WM. The relative high Dice ratio in GM might be due to the slight over-segmentation of GM. The inter-rater Dice ratio is 0.88±0.01 for GM, and 0.87±0.02 for WM. The higher Dice ratio between the two manual raters might attribute to the use of the same initial segmentation in the beginning of their manual delineation.

Volume error is also calculated to evaluate the segmentation performance. The volume error in the GM is 0.05±0.02 with rater 1, 0.12±0.06 with rater 2, and the inter-rater volume error is 0.09±0.07. For WM, the volume error is 0.10±0.05 with rater 1, 0.18±0.07 with rater 2, and the inter-rater volume error is 0.10±0.07. It can be seen that the volume error by the proposed method is comparable with inter-rater difference.

4. CONCLUSION

We presented a method for performing brain tissue segmentation of neonatal brain images by using a subject-specific probabilistic atlas. This method takes advantage of the available longitudinal data in our study, i.e., using the segmentation results from the images acquired at a later time to guide the segmentation of the images acquired at earlier times. The experimental results demonstrated that the proposed method have potential to achieve promising segmentation results for the neonate images.

To further improve the performance of the proposed method, we are now exploring in two directions. First, we are investigating an integrated method to combine the non-rigid registration with tissue segmentation, particularly to use non-rigid registration algorithms to align the subject-specific atlas with the intermediate segmentation results at each iteration, aiming to improve the registration and segmentation performance simultaneously. Second, we are investigating the advantage of combining the probabilistic atlases from two years old and one year old, to produce better segmentations on the neonate images.

REFERENCES

[1]. Gerig G, Davis B, Lorenzen P, et al. Computational Anatomy to Assess Longitudinal Trajectory of Brain Growth. 3DPVT 2006. 2006:1041–1047.

[2]. Knickmeyer RC, Gouttard S, Kang C, et al. A structural MRI study of human brain development from birth to 2 years. J Neurosci. 2008; 28(47):12176–12182. [PubMed: 19020011]

[3]. Dubois J, Benders M, Cachia A, et al. Mapping the Early Cortical Folding Process in the Preterm Newborn Brain. Cerebral Cortex. 2008; 18(6):1444–1454. [PubMed: 17934189]

[4]. Pham DL, Xu C, Prince JL. A survey of current methods in medical image segmentation. Annual Review of Biomedical Engineering. 2000; 2:315–337.

[5]. Connors SL, Levitt P, Matthews SG, et al. Fetal mechanisms in neurodevelopmental disorders. Pediatr Neurol. 2008; 38(3):163–176. [PubMed: 18279750]

[6]. Song Z, Awate SP, Licht DJ, et al. Clinical neonatal brain MRI segmentation using adaptive nonparametric data models and intensity-based Markov priors. MICCAI 2007. 2007; 10:883–890.

[7]. Nishida M, Makris N, Kennedy DN, et al. Detailed semiautomated MRI based morphometry of the neonatal brain: preliminary results. Neuroimage. 2006; 32(3):1041–1049. [PubMed: 16857388]

[8]. Prastawa M, Gilmore JH, Lin W, et al. Automatic segmentation of MR images of the developing newborn brain. Medical Image Analysis. 2005; 9(5):457–466. [PubMed: 16019252]

[9]. Xue H, Srinivasan L, Jiang S, et al. Automatic segmentation and reconstruction of the cortex from neonatal MRI. Neuroimage. 2007; 38(3):461–477. [PubMed: 17888685]

[10]. Weisenfeld NI, Mewes AU, Warfield SK. Highly accurate segmentation of brain tissue and subcortical gray matter from newborn MRI. MICCAI 2006. 2006; 9:199–206.

[11]. Pham DL, Prince JL. An adaptive fuzzy C-means algorithm for image segmentation in the presence of intensity inhomogeneities. Pattern Recognition Letters. 1999; 20(1):57–68.

[12]. Bazin PL, Pham DL. Topology-Preserving Tissue Classification of Magnetic Resonance Brain Images. IEEE Transactions on Medical Imaging. 2007; 26(4):487–496. [PubMed: 17427736]

[13]. Joshi S, Davis B, Jomier M, et al. Unbiased diffeomorphic atlas construction for computational anatomy. Neuroimage. 2004; 23:151–160.

[14]. Altaye M, Holland SK, Wilke M, et al. Infant brain probability templates for MRI segmentation and normalization. Neuroimage. 2008; 43(4):721–730. [PubMed: 18761410]

[15]. Thomas, B. T. Yeo; Sabuncu, MR.; Desikan, R., et al. Effects of registration regularization and atlas sharpness on segmentation accuracy. Medical Image Analysis. 2008; 12(5):603–615. [PubMed: 18667352]

[16]. Shattuck DW, Leahy RM. Automated graph-based analysis and correction of cortical volume topology. IEEE Transactions on Medical Imaging. 2001; 20(11):1167–1177. [PubMed: 11700742]

[17]. Sled JG, Zijdenbos AP, Evans AC. A nonparametric method for automatic correction of intensity nonuniformity in MRI data. IEEE Transactions on Medical Imaging. 1998; 17(1):87–97. [PubMed: 9617910]

[18]. Zhang Y, Brady M, Smith S. Segmentation of brain MR images through a hidden Markov random field model and the expectation-maximization algorithm. IEEE Transactions on Medical Imaging. 2001; 20(1):45–57. [PubMed: 11293691]

[19]. Ashburner J, Friston KJ. Unified segmentation. Neuroimage. 2005; 26(3):839–851. [PubMed: 15955494]

[20]. Yushkevich PA, Piven J, Hazlett HC, et al. User-guided 3D active contour segmentation of anatomical structures: Significantly improved efficiency and reliability. Neuroimage. 2006; 31(3):1116–1128. [PubMed: 16545965]

[21]. Dice LR. Measures of the Amount of Ecologic Association Between Species. Ecology. 1945; 26(3):297–302.

[22]. Zijdenbos AP, Dawant BM, Margolin RA, et al. Morphometric analysis of white matter lesions in MR images: methodand validation. IEEE Transactions on Medical Imaging. 1994; 13(4):716–724. [PubMed: 18218550]

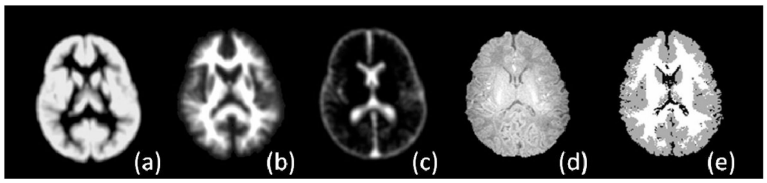

Fig. 1.

Segmentation of neonatal brain images using a population-based tissue probabilistic atlas, as shown in (a-c). The original neonatal brain image and its segmentation result are shown in (d) and (e), respectively.

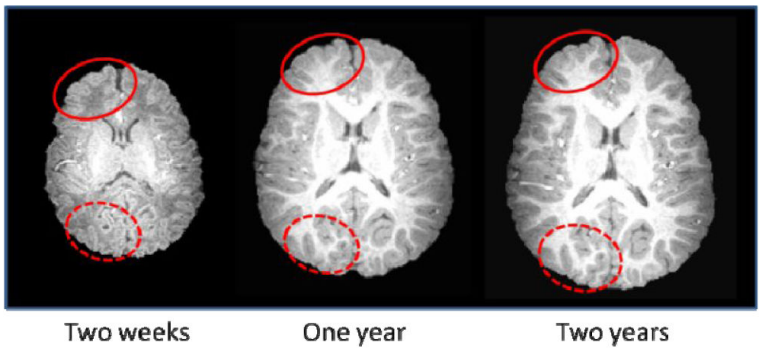

Fig. 2.

Demonstration of the similarity of the cortical convolution patterns in images acquired from a subject imaged at two weeks, one year old, and two years old. Red circles are provided for an easy comparison of the same local cortical folds across different times.

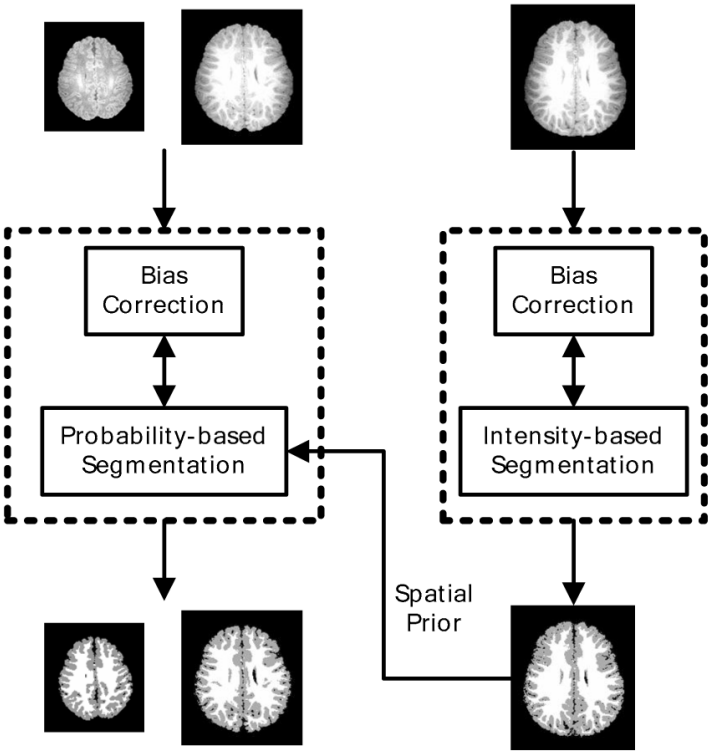

Fig. 3.

The proposed tissue segmentation framework. The images in the top row are the original T1-weighted MR images acquired at approximately two weeks, one year old, and two years old. The images in the bottom row are the corresponding segmentation results.

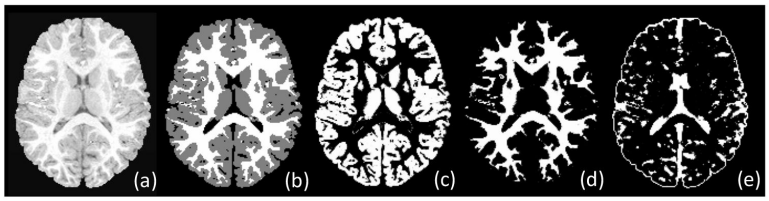

Fig. 4.

Tissue segmentation results for images obtained from a representative two-year-old. (a) Original T1-weighted image, (b) tissue segmentation result, and (c-e) probabilistic maps of GM, WM, and CSF.

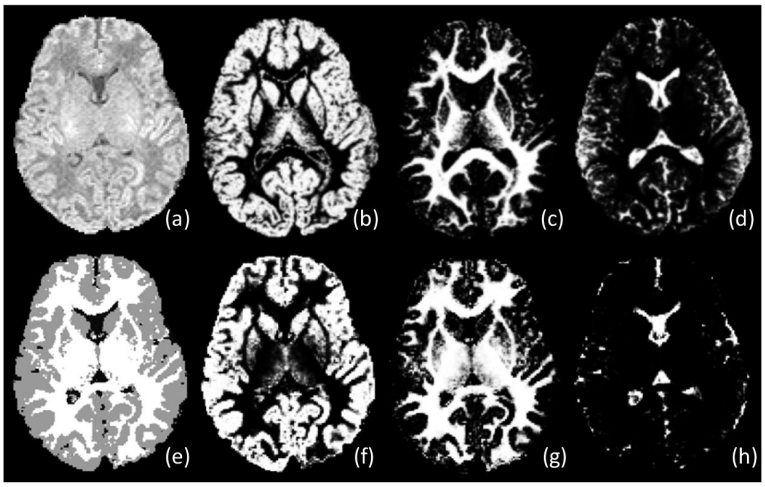

Fig. 5.

Illustration of prior and posterior probability maps. (a) Original T1-weighted image; (b-d) the warped prior probabilistic maps of GM, WM, and CSF, warped from the later-time image; (e) segmentation result, integrated from the posterior probability maps of GM, WM, and CSF in (f-h), respectively.

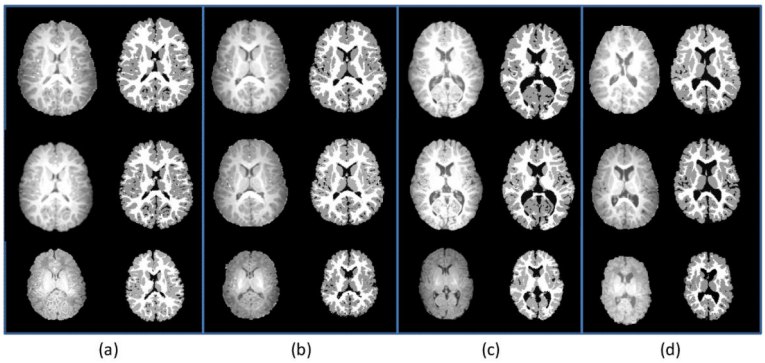

Fig. 6.

Segmentation results of longitudinal images from four subjects, corresponding to the panels in (a-d), respectively. For each subject, from top to bottom are the two-year-old, one-year, and two-week images, and from left to right are the original skull-stripped images and the segmentation results.

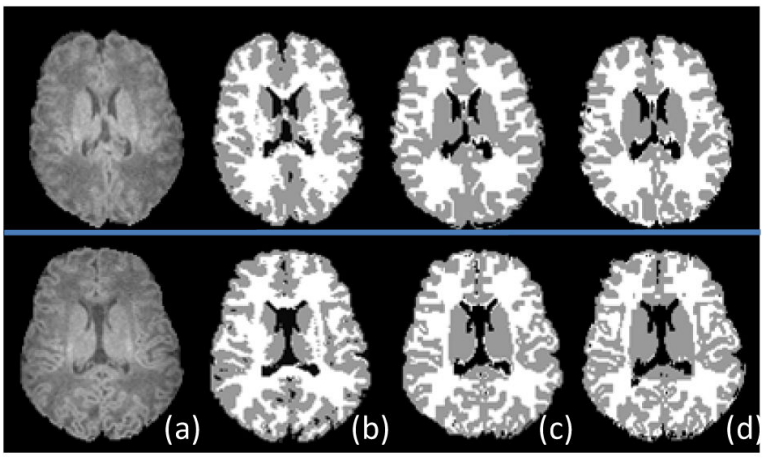

Fig. 7.

Segmentation results of two neonates (top and bottom) by our proposed method and two manual raters. (a) Original T1-weighted images; (b) Segmentation results by our proposed method; (c-d) Manual segmentation results by two experts.

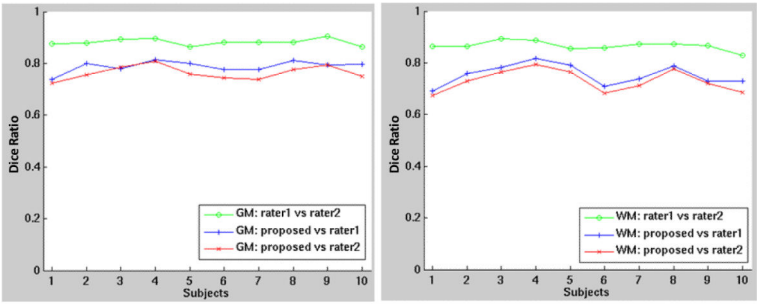

Fig. 8.

Evaluation of segmentation results between manual raters and our proposed methods with the Dice ratio. The left panel is the result for GM, and the right panel is for WM.